Models of spherical and rectangular cuboid loudspeaker arrays

Franz Zotter, Hannes Pomberger

Institute of Electronic Music and Acoustics

University of Music and Performing Arts Graz, Austria

zotter@iem.at, pomberger@iem.at

Abstract

Compact spherical/cubical loudspeaker arrays are used as beamformers to radiate focused sound with adjustable direction. A common enclosure housing all the transducers is easier to manufacture but acoustically couples their motion, which appears to make their independent control more challenging. However, simple analytic IIR filters to control cubical arrays were recently published and motivate the effort to investigate their existence for more general common-enclosure arrays in the future. This contribution describes the analytic model of the interior crosstalk in (i) rectangular cuboid enclosures housing multiple piston-shape transducers and (ii) in spherical enclosures housing multiple cap-shape transducers. For both models, this contribution shows the accurate integrals over the interior modes that evaluate both the contribution of the transducers' velocity boundary conditions and the forces by which the produced pressure loads on active/passive transducers. A fully causal model is obtained by assuming a damping constants for the interior modes. Both models are demonstrated and for the cuboid model, the full electro-acoustic model is shown to compare well to laser velocity measurements on a physical prototype. This verifies the model up to frequencies at which transducers break up into partial vibrations. Higher-order interior modes often become irrelevant, as at high frequencies the transducer mass starts to dominate. Simple, well-calibrated IIR control appear feasible, in general.

Keywords: acoustic coupling, common-enclosure cube/sphere loudspeaker arrays, cross-talk cancellation

1 INTRODUCTION

Sphere- and cube-shaped or platonic loudspeaker arrays have been discussed in various papers [3, 12, 5, 2, 13, 10, 9, 7, 1, 14, 11] that established the electroacoustic background and technology required to describe compact spherical loudspeaker arrays built with electrodynamic transducers, in order to drive them with superdirectional beamforming.
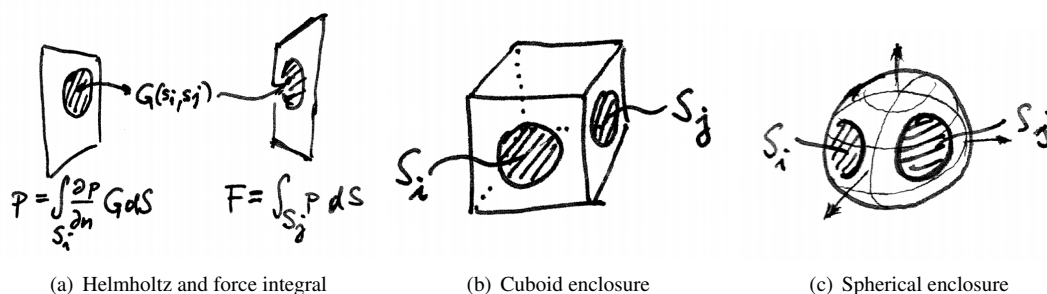

(a) Helmholtz and force integral (b) Cuboid enclosure (c) Spherical enclosure

Figure 1. The coupling forces between sending and a receiving parts of a coboid or spherical enclosure are evaluated as impedance matrix using the Helmholtz integral over the vibrating surface S_i and the resulting force from the integrated pressure load on the receiver surface S_j.

This work is inspired by the simple analytic models that works for a 4-channel horizontally beamforming loud-

speaker cube [4], and it refines the models [13, 9, 7]. This is done with the purpose to simplify velocity control, and might yield simple time-domain multichannel filters to digitally equalize the transducer velocities and remove the cross talk of the interior acoustic coupling.

Based on the refined model and measurements, we can show which model parts are often negligible (e.g. higher interior modes) or would be much effort for limited benefit (modal break up of the loudspeaker cone vibration).

2 ACOUSTIC COUPLING BETWEEN RIGID ENCLOSURE PARTS

The motion of transducers mounted on a common enclosure is coupled by the impedance $Z_{a,ij}$

$$F_j = \sum_i Z_{a,ij} v_i. \tag{1}$$

that yields a force F_j due to any transducer velocity v_i. To get the impedance, $Z_{a,ij}$, we calculate the force on a resting, piston-shaped interior surface part S_j by the integral $F_{ij} = \int_{S_j} p(\boldsymbol{s}_j) \mathrm{d}\boldsymbol{s}_j$ of the sound pressure $p(\boldsymbol{s}_j)$ loading on S_j. The integrated sound pressure $p(\boldsymbol{s}_j)$ is caused by a piston-shaped surface part S_i vibrating with the velocity v_i. It results from the Helmholtz integral $p(\boldsymbol{s}_j) = \int_{S_i} \frac{\partial p}{\partial n} G \mathrm{d}\boldsymbol{s}_i = \mathrm{i}\omega\rho\, v_i \int_{S_i} G \mathrm{d}\boldsymbol{s}_i$ using the interior-problem Neumann Green's function $G(\boldsymbol{s}_i - \boldsymbol{s}_j)$. This function is observed at $\boldsymbol{x}$ with a source at $\boldsymbol{x}_0$, and it is defined by the non-homogeneous Helmholtz equation with the wave number $k = \frac{\omega}{c}$

$$(\triangle + k^2) G = -\delta^3(\boldsymbol{x} - \boldsymbol{x}_0), \tag{2}$$

and G fulfills the boundary condition $\frac{\partial G}{\partial n(\boldsymbol{s})} = 0$ everywhere perpendicular to the given enclosure $\boldsymbol{s} \in S$. It is composed of interior modes $G = \sum_{lmn} \gamma\, \psi_{lmn}(\boldsymbol{x})$. These interior modes are countable, have 3 indices in 3D, they are orthogonal (normalized) $\iiint \psi_{l'm'n'}(\boldsymbol{x}) \psi_{lmn}(\boldsymbol{x}) \mathrm{d}^3\boldsymbol{x} = \delta_{ll'} \delta_{mm'} \delta_{nn'}$ eigenfunctions to the Laplacian $\triangle \psi_{lmn} = -k_{lmn}^2 \psi_{lmn}$, with the real-valued wave number k_{lmn}^2 as eigenvalue. The required modes and their eigenvalues support the homogeneous normal velocity boundary conditions $v_n = \frac{\mathrm{i}}{\omega\rho} \frac{\partial \psi_{lmn}(\boldsymbol{s})}{\partial n(\boldsymbol{s})} = 0$ everywhere on the enclosure $\boldsymbol{s} \in S$. Inserted into the Helmholtz equation $\sum_{lmn}(k^2 - k_{lmn}^2)\, \gamma\, \psi_{lmn}(\boldsymbol{x}) \mathrm{d}^3\boldsymbol{k} = -\delta^3(\boldsymbol{x} - \boldsymbol{x}_0)$ and using orthonormality by multiplication with $\psi_{l'm'n'}$ and integration over $\boldsymbol{x}$, the unknown coefficient becomes $\gamma = -\frac{\psi_{l'm'n'}(\boldsymbol{x}_0)}{k^2 - k_{lmn}^2}$ so that Green's function becomes

$$\Rightarrow G(\boldsymbol{x} - \boldsymbol{x}_0) = -\sum_{lmn} \frac{\psi_{lmn}(\boldsymbol{x})\, \psi_{lmn}(\boldsymbol{x}_0)}{k^2 - k_{lmn}^2} = -\lim_{\sigma_{lmn} \to {}^+0} c^2 \sum_{lmn} \frac{\psi_{lmn}(\boldsymbol{x})\, \psi_{lmn}(\boldsymbol{x}_0)}{(\omega - \mathrm{i}\sigma_{lmn})^2 - \omega_{lmn}^2}. \tag{3}$$

A mode-specific positive and real damping constant σ_{lmn} has been introduced for a causal solution.

Coupling forces: Apart from obtaining problem-specific modes ψ_{lmn}, obtaining the coupling impedance $Z_{a,ij}$ requires to integrate the source mode $\psi_{lmn}(\boldsymbol{s}_i)$ over S_i and the field mode $\psi_{lmn}(\boldsymbol{s}_j)$ over S_j

$$F_j = -\sum_i v_i \sum_{lmn} \frac{\mathrm{i}\omega\rho c^2 \int_{S_i} \psi_{lmn}(\boldsymbol{s}_i)\, \mathrm{d}\boldsymbol{s}_i \int_{S_j} \psi_{lmn}(\boldsymbol{s}_j)\, \mathrm{d}\boldsymbol{s}_j}{(\omega - \mathrm{i}\sigma_{lmn})^2 - \omega_{lmn}^2} = -\sum_i v_i \sum_{lmn} Z_{a,ij}^{(lmn)} = \sum_i v_i Z_{a,ij}. \tag{4}$$

Lower modes integrate to a sample-and-weight approximation $\lim_{lmn \to 0} \int_S \psi_{lmn}(\boldsymbol{s}) \mathrm{d}\boldsymbol{s} = -\psi_{lmn}(\boldsymbol{x}) \int_S \mathrm{d}\boldsymbol{s} = \psi_{lmn}(\boldsymbol{x}) A$ because they do not vary much over position

$$\lim_{lmn \to 0} Z_{a,ij}^{(lmn)} = -\frac{\mathrm{i}\omega\rho c^2\, \psi_{lmn}(\boldsymbol{x}_i) A_i A_j\, \psi_{lmn}(\boldsymbol{x}_j)}{(\omega - \mathrm{i}\sigma_{lmn})^2 - \omega_{lmn}^2}. \tag{5}$$

Without approximation, the constant 0 Hz mode $\psi_{000} = \sqrt{V}^{-1}$, $\omega_{lmn} = 0$ responds with the impedance to the transducer velocity, with the known stiffness $\frac{\rho c^2 A^2}{V}$, and for simplicity $\sigma_{000} = 0$,

$$Z_{a,ij}^{(000)} = -\frac{\mathrm{i}\omega\rho c^2 A_i A_j}{\omega^2 V} = \frac{\rho\, c^2 A_i A_j}{\mathrm{i}\omega V}. \tag{6}$$

2.1 Acoustic coupling between vibrating pistons of a rectangular cuboid enclosure

The interior modes for a rigid cuboid rectangular box uses cosine modes with corresponding wave numbers k_{lmn}

$$\psi_{lmn}(\boldsymbol{x}) = \frac{\cos(\frac{\pi}{L_x}lx)\cos(\frac{\pi}{L_y}my)\cos(\frac{\pi}{L_z}nz)}{\sqrt{L_x L_y L_z (2-\delta_l)^{-1}(2-\delta_m)^{-1}(2-\delta_n)^{-1}}}, \qquad k_{lmn}^2 = (\tfrac{\pi}{L_x}l)^2 + (\tfrac{\pi}{L_y}m)^2 + (\tfrac{\pi}{L_z}n)^2,$$

and ensure zero-velocity boundaries $\frac{\partial \psi_{lmn}}{\partial x}\big|_{x=0,L_x} = \frac{\partial \psi_{lmn}}{\partial y}\big|_{y=0,L_y} = \frac{\partial \psi_{lmn}}{\partial z}\big|_{z=0,L_z} = 0$, $l,m,n \in \mathbb{N}_0$. Appendix A solves the integrals of the modes $\psi(\boldsymbol{x})$ over both the emitting and receiving piston.

Solution: For evaluation at constant z and excitation at constant x, for instance, assuming a piston radius R_p, we get the modal coupling impedance $Z_{\mathrm{a},ij}^{(lmn)}$ with all scalars and constants ($\omega_{lmn} = k_{lmn}c$)

$$Z_{\mathrm{a},ij}^{(lmn)} = -\frac{\mathrm{i}\omega\rho c^2\, \psi_{lmn}(\boldsymbol{x}_i) \dfrac{2R_\mathrm{p} J_1\left(\pi R_\mathrm{p}\sqrt{(\frac{l}{L_x})^2+(\frac{m}{L_y})^2}\right)}{\sqrt{(\frac{l}{L_x})^2+(\frac{m}{L_y})^2}} \dfrac{2R_\mathrm{p} J_1\left(\pi R_\mathrm{p}\sqrt{(\frac{m}{L_y})^2+(\frac{n}{L_z})^2}\right)}{\sqrt{(\frac{m}{L_y})^2+(\frac{n}{L_z})^2}} \psi_{lmn}(\boldsymbol{x}_j)}{(\omega - \mathrm{i}\sigma_{lmn})^2 - \omega_{lmn}^2}. \tag{7}$$

The sample-and-weight approximation for low orders / small arguments $J_1(x) \approx \frac{x}{2}$ verifies the solution by approaching Eq. (5) for both modal multipliers; exemplarily: $\lim_{lm\to 0} \dfrac{2R_\mathrm{p} J_1\left(R_\mathrm{p}\pi\sqrt{(\frac{l}{L_x})^2+(\frac{m}{L_y})^2}\right)}{\sqrt{(\frac{l}{L_x})^2+(\frac{m}{L_y})^2}} = \pi R_\mathrm{p}^2 = A$.

2.2 Acoustic coupling between between vibrating caps of a spherical enclosure

The acoustic coupling in a spherical enclosure works similar as above, but uses interior modes of a sphere, a direction vector $\boldsymbol{\theta}$, the variable radius r and R is the radius of the enclosure,

$$\psi_{lmn}(\boldsymbol{x}) = N_{ln} Y_n^m(\boldsymbol{\theta})\, j_n(k_{ln}r), \qquad \text{with } k_{lmn} = k_{ln} \text{ such that } j_n'(k_{ln}R) = 0. \tag{8}$$

The spherical harmonics $Y_n^m(\boldsymbol{\theta})$ are orthonormal $\int_{\mathbb{S}^2} Y_n^m Y_{n'}^{m'} \mathrm{d}\boldsymbol{\theta} = \delta_{nn'}^{mm'}$, and the orthogonal spherical Bessel fucntions $j_n(k_{ln}r)$ are normalized by N_{ln} as derived in Appendix B. The wave numbers k_{ln} need to be found to as roots of $j_n'(k_{ln}R) = 0$ to fulfill the boundary conditions; $l,n,m \in \mathbb{N}_0$ with $0 \le n$, $|m| \le n$, and l counts the zeros of $j_n'(k_{ln}R) = 0$ upwards. Non-trivial modes $j_n(k_{ln}r) \ne 0$ exist for $n=0,1$ using $l \ge 0$, and $n>1$ with $l \ge 0$.

Spherical cap function: The integral of $Y_n^m(\boldsymbol{\theta})$ over a spherical cap at the radius R is known to be $R^2 Y_n^m(\theta_0)\, a_n$

$$a_n = 2\pi \begin{cases} \dfrac{\cos\frac{\alpha}{2} P_n(\cos\frac{\alpha}{2}) - P_{n+1}(\cos\frac{\alpha}{2})}{n}, & \text{for } n>0 \\ 1 - \cos\frac{\alpha}{2}, & \text{for } n=0. \end{cases} \tag{9}$$

Solution: The response is of the same structure as for the cuboid, only the middle part with the cap shapes is now exactly square and contains the term $N_{ln}^2 j_n(k_{ln}R)^2 R^3$ Eq. (23) (shorthand $N_{ln}^2 j_n(k_{ln}R)^2 R^3 = \frac{(2+\delta_l)(k_{ln}R)^2}{(k_{ln}R)^2 - n(n+1)}$)

$$Z_{\mathrm{a},ij}^{(lmn)} = -\frac{\mathrm{i}\omega\rho c^2 Y_n^m(\boldsymbol{\theta}_i)\left[\frac{(a_n R^2)^2}{R^3}\left(N_{ln}^2 j_n(k_{ln}R)^2 R^3\right)\right] Y_n^m(\boldsymbol{\theta}_j)}{(\omega - \mathrm{i}\sigma_{ln})^2 - \omega_{ln}^2}; \tag{10}$$

summation over m could be further simplified by $\sum_m Y_n^m(\boldsymbol{\theta}_i) Y_n^m(\boldsymbol{\theta}_j) = \frac{2n+1}{4\pi} P_n(\boldsymbol{\theta}_i^\mathrm{T}\boldsymbol{\theta}_j)$. App. B Eq. (25) verifies a sample-and-weight approximation $[a_n R^2]^2 = [2\pi R^2(1 - \cos\frac{\alpha}{2})]^2 = A^2$ for $\alpha \to 0$, which yields with the spherical volume $\frac{1}{R^3} = \frac{4\pi}{3V}$ and the shorthand normalizer $Z_{\mathrm{a},ij}^{(lmn)} = -\frac{\mathrm{i}\omega\rho c^2}{(\omega - \mathrm{i}\sigma_{ln})^2 - \omega_{ln}^2} Y_n^m(\boldsymbol{\theta}_i) \frac{4\pi A^2}{3V}\left[\frac{(2+\delta_l)(k_{ln}R)^2}{(k_{ln}R)^2 - n(n+1)}\right] Y_n^m(\boldsymbol{\theta}_j)$. For the zeroth-order mode $(Y_0^0)^2 = \frac{1}{4\pi}$ this approximation is exact. For the modal frequency $\omega_{00} = 0$ of $l=0$ with $\sigma_{00} = 0$, the square brackets yields 3, and we get the known stiffness $Z_{\mathrm{a},ij}^{(000)} = -\frac{\mathrm{i}\omega\rho c^2 A^2}{\omega^2 V} = \frac{1}{\mathrm{i}\omega}\frac{\rho c^2 A^2}{V}$.

parameter	value	unit	parameter	value	unit
coil resistance R_c	$3.2 \cdot 1$	Ω	coil inductance L_c	$0.6 \cdot 10^{-3}$	H
transduction constant Bl	$4.4 \cdot 1$	Tm			
effective piston area A	$129 \cdot 10^{-4}$	m^2	dynamically moved mass M_m	$12 \cdot 10^{-3}$	kg
equivalent volume V_m	$38 \cdot 10^{-3}$	m^3	$\rightarrow$ stiffness $S_\mathrm{m} = \rho c^2 A^2 / V_\mathrm{m}$	$618 \cdot 1$	N/m
mechanical Q factor Q_m	$2.16 \cdot 1$	-	$\rightarrow$ damping $R_m = \sqrt{M_\mathrm{m} S_\mathrm{m}}/Q$	$1.26 \cdot 1$	Ns/m
edge length L_xyz	$22 \cdot 10^{-2}$	m	$\rightarrow$ volume $V = L_\mathrm{xyz}^3$	$10.6 \cdot 10^{-3}$	m^3
$\rightarrow$ sphere radius $R = \sqrt[3]{3V/4\pi}$	$13.7 \cdot 10^{-2}$	m			
$\rightarrow$ piston radius $R_\mathrm{p} = \sqrt{A/\pi}$	$6.4 \cdot 10^{-2}$	m	$\rightarrow$ cap size $\alpha = 2\arccos\left(1 - A/2\pi R^2\right)$	$54°$	

Table 1. Electro-acoustic characteristics of the loudspeaker cube with Visaton WS170S 4Ohm transducers.

3 CROSS-TALK AND VELOCITY CONTROL: ELECTROACOUSTIC MODEL

Compact spherical loudspeaker array literature [13, 9, 8, 4] describes radiation as caused and controlled by the boundary condition that the housing and transducer velocities v_j impose. Transducers are fed by voltages, therefore directivity/radiation control seeks the driving voltages U_i able to synthesize transducer velocities v_j in a desired constellation. We complement the acoustic coupling from above with a complete electro-acoustic model. As outlined in [4, 8], the transducer voltage corresponds to its current times impedance (static-coil impedance $Z_{\mathrm{c},i}$ consists of inductance and resistance) plus the voltage induced by the transducer's velocity (we use $s = i\omega$)

$$U_i = Z_{\mathrm{c},i} I_i + U_{\mathrm{ind},i}, \qquad \text{with } Z_{\mathrm{c},i} = R_{\mathrm{c},i} + L_{\mathrm{c},i}s. \tag{11}$$

Induction by velocity and the relation between current and force are described by the transduction constant Bl_i

$$F_i = Bl_i I_i, \qquad \text{and } U_{\mathrm{ind},i} = Bl_i v_i, \tag{12}$$

and the force is proportional to the mechanical transducer impedance ($Z_{\mathrm{m},i}$, mass, damping, and stiffness)

$$F_i = Z_{\mathrm{m},i} v_i + F_{\mathrm{a},i}, \qquad \text{with } Z_{\mathrm{m},i} = M_{\mathrm{m},i}s + R_{\mathrm{m},i} + S_{\mathrm{m},i}s^{-1} \tag{13}$$

plus the acoustic force $F_{\mathrm{a},i}$ loading on the transducer, which couples the transducer velocities, see Eq. (4),

$$F_{\mathrm{a},i} = \sum_{j=1}^{\mathrm{L}} Z_{\mathrm{a},ij} v_j. \tag{14}$$

The exterior acoustic impedance is typically negligible and therefore disregarded. Altogether, we get a system mapping the desired output velocities to the required input voltages

$$U_i = Z_{\mathrm{c},i} I_i + U_{\mathrm{ind}}, i = Z_{\mathrm{c},i} \frac{F_i}{Bl_i} + Bl_i v_i = Z_{\mathrm{c},i} Bl_i^{-1} \left(Z_{\mathrm{m},i} v_i + \sum_j Z_{\mathrm{a},ij} v_j \right) + Bl_i v_i \tag{15}$$

$$= \sum_j \left[Bl_i \delta_{ij} + Z_{\mathrm{c},i} Bl_i^{-1} Z_{\mathrm{m},i} \delta_{ij} + Z_{\mathrm{c},i} Bl_i^{-1} \left(\sum_{lmn} Z_{\mathrm{a},ij}^{(lmn)} \right) \right] v_j.$$

Stacking velocities and voltages into vectors $\boldsymbol{v} = [v_j]$, $\boldsymbol{u} = [U_i]$, and transduction factors into a matrix $\boldsymbol{C} = [Bl_i \delta_{ij} + Z_{\mathrm{c},i} Bl_i^{-1} Z_{\mathrm{m},i} \delta_{ij} + Z_{\mathrm{c},i} Bl_i^{-1} \sum_{lmn} Z_{\mathrm{a},ij}^{(lmn)}]_{ij}$, we write the multiple-input-multiple-output system (MIMO) compactly as $\boldsymbol{u} = \boldsymbol{C}\boldsymbol{v}$. Of the acoustical Eq. (4), electrical Eq. (11), and mechanical impedances Eq. (13), the cross-talk-cancelling, velocity-controlling MIMO system $\boldsymbol{C}$ only contains parallel combinations, i.e. causal, parallel filters. Consequently, if all electro-acoustic components $R_{\mathrm{c},i}$, $L_{\mathrm{c},i}s$, $(=Z_{\mathrm{c},i})$, $M_{\mathrm{m},i}$, $R_{\mathrm{m},i}$, $S_{\mathrm{m},i}$, $(=Z_{\mathrm{m},i})$, Bl_i, $Z_{\mathrm{a},i}$, α, R a, V, σ_{lmn} are identified, we get a well-defined control system delivering the voltages $\boldsymbol{u}$ required to obtain the desired velocities $\boldsymbol{v}$. It can directly be implemented, as is, by parallel, digital IIR filters.

4 EXPERIMENTAL STUDY: CUBOID AND SPHERE ARRAY

To inspect the coupling and electro-acoustic model, we consider a concrete example geometry based on an IEM loudspeaker cube [6, 4]. It houses transducers at $0°$, $90°$, $180°$, $-90°$ in azimuth at zero elevation. First we inspect the coupling model assuming either a cube housing or an equivalent-volume sphere housing (with equivalent-piston-area cap sizes). Tab 1 specifies the parameters.

Fig. 2 shows the frequency response of the force F_1. The geometry and parameters are $L_x = L_y = L_z = 23$ cm (cube), radius 14.3 cm (sphere), piston $R_p = 6.4$ cm, $\rho = 1.2$, $c = 343$, $\sigma_{lmn} = \frac{1+\omega_{lmn}/(2\pi300)}{0.14} 3\ln 10$. Monopole $[v_i] = [1,1,1,1]$, dipole $[v_i] = [1,0,-1,0]$ and quadrupole $[v_i] = [1,-1,1,-1]$ velocity patterns were inserted, modes used up to 15 kHz and maximum indices of the simulated modes were N $= 18$. Regardless of the cube or sphere enclosure: Between simplified sample-and-weight Eq. (5) (left) and proper piston/cap-integrals Eq. (7)/(10) (right), differences are drastic: Bessel-function/sphere-cap factors attenuate higher-order modes and reduce their long low-frequency skirts, which is more accurate if assuming piston/cap loudspeakers. At 0 Hz, only the velocity monopole pattern is loaded by volume stiffness $Z_{a,ij}^{(000)}$, therefore equivalent cube/sphere volumes and equivalent piston/cap areas were chosen for easy comparison. The high-frequency amplitude drop for the sphere enclosure stems from the limit $kR < $ N at 6.3 kHz, i.e. N $= 18$ was chosen slightly too low.
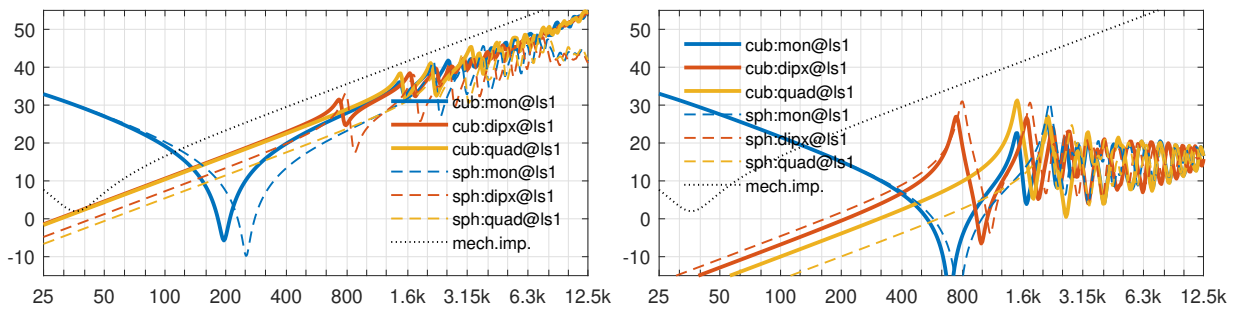

Figure 2. Frequency response in dB of the acoustic coupling force F_1 at the first transducer of four (horizontally every $90°$) of a loudspeaker cube (solid) or equivalent-volume sphere (dashed) for specific velocity patterns: monopole (*mon*), dipole in x direction (*dipx*), or quadrupole (*quad*); the dotted response is the added force of the mechanical load Z_m Eq. (13) for transducers of Tab. 1. The left response considers a simplified sample-and-weight solution, the right one uses proper Bessel-function/sphere-cap factors.

For the cube housing, we compare the electro-acoustic model with open Laser-Doppler vibrometry measurements[1] of the transducer velocities when driving every single input voltage of a multi-channel amplifier.

It is important to note that the measurements of the loudspeaker cube contains a 101 Hz, 3rd order Butterworth high pass of the Laser vibrometer that was removed from the responses shown below. When transformed to the DFT domain, the measurements describe the inverse control system at every frequency bin $u = T v$. This matrix T^{-1} is inverted to obtain the control system C_{meas} at every frequency bin, which is comparable to the model C. Figure 3 compares measurement and model in terms of the voltage frequency response of the first of the loudspeaker cube's input channels, when desiring different velocity patterns as in the simulation above.

The comparison is done either when using only the first mode at 0 Hz (left) or all the interior modes up to 15 kHz (right). It becomes clear that above 800 Hz, the required voltages drops considerably, when compared to the model. Obviously the loudspeaker does not exhibit the mechanical-impedance related rise by $L_c M_m s^2/Bl$, cp. Fig. 2. This happens as the transducer cone does not move as a solid mass anymore, and 800 Hz appears to be the modal break-up frequency of the cone. Above this frequency, precise modeling would be difficult, but is also unimportant for beamforming that only requires precision below the spatial aliasing limit, i.e. $f < 746$ kHz.
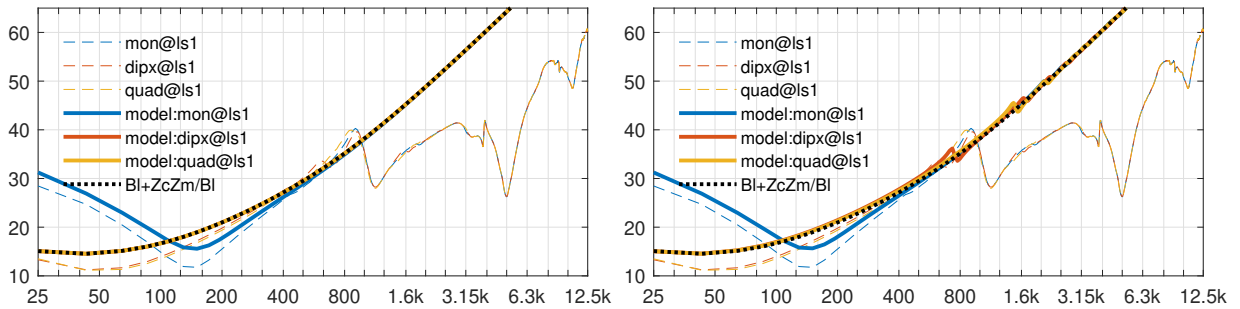
---

[1] http://phaidra.kug.ac.at/o:67626

Figure 3. Model voltages of the loudspeaker cube array in dB over frequency, when the array is driven in the velocity patterns $[1,1,1,1]$ (monopole, *mon*), $[1,0,-1,0]$ (dipole in *x* direction, *dipx*), or $[1,-1,1,-1]$ (quadrupole, *quad*), compared to the frequency-domain matrix-inverted velocity measurements from voltages. left: acoustic crosstalk only considers 0 Hz compression mode, right: all the modes up to 15 kHz. Above 800 Hz the loudspeaker cone oscillates in partial vibrations.

Between 300 and 800 Hz, the required voltage is modeled sufficiently well by the acoustic system without coupling. The mode at 746 Hz, see Fig. 2 (right), obviously does not have much influence (2dB on the dipole response in measurement and model, between 600 Hz and 800 Hz). In this regard, the simple impedance coupling of only the 0 Hz mode Eq. (6) without any further term is sufficient, as in [8, 4] and Fig 2 (left).

The remaining deviations between model and measurement below 200 Hz that amount to a couple of dB are not explained well, however the model parameters from the technical specifications were not individually tuned.

5   CONCLUSION

This work demonstrated how to analytically model physical acoustic forces coupling multiple loudspeakers whose back sides are connected via the common cuboidal Eq. (7) or spherical enclosure Eq. (10).

For most cases, a drastic simplification will be sufficient as in [8, eq.31]: the most relevant mode to consider is the 0 Hz compression mode Eq. (6) of the air enclosed. It yields the known volume stiffness as impedance $Z_{ij} = \frac{i\rho c^2 A_i A_j}{i\omega V}$ of the acoustic coupling, to which the net of all surface-weighted loudspeaker velocities contribute constructively/destructively. This is because at frequencies above the loudspeaker resonance frequency, the transducer mass dominates the impedances, what makes coupling by higher modes negligible.

The full electro-acoustic model for frequencies below which the loudspeaker cone breaks up into partial vibrations promises a full, causal, feed-forward IIR transducer velocity control, without the need for MIMO system inversion. However it is assumed that transducer and enclosure parameters need to be identified accurately and individually than given in the specificantions, when employed in superdirectional beamformers.

In addition to the electro-acoustic components requiring a third-order control system for every transducer, the acoustic compression mode increases the system order by one and couples the transducers at low frequencies.

REFERENCES

[1] R. M. Aarts and A. J. Jannsen. Comparing sound radiation from a loudspeaker with that from a flexible spherical capon a rigid sphere. *J. Audio Eng. Soc.*, 59(4):201–212, 2011.

[2] R. Avizienis, A. Freed, P. Kassakian, and D. Wessel. A compact 120 independent element spherical loudspeaker array with programmable radiation patterns. In *prepr. 6783, 120th AES Conv.*, Paris, May 2006.

[3] J. L. Butler and S. L. Ehrlich. Superdirective spherical radiator. *J Acoust. Soc. Am.*, 61(6):1427–1431, 1977.

[4] T. Deppisch, N. Meyer-Kahlen, F. Zotter, and M. Frank. Surround with depth on first-order beam-controlling loudspeakers. In *prepr. 9977, 144th AES Conv.*, May 2018.

[5] P. Kassakian and D. Wessel. Characterization of spherical loudspeaker arrays. In *prepr. 1430, AES Conv*, San Francisco, CA, 2004.

[6] N. Meyer-Kahlen, K. Pollack, and F. Zotter. Design and measurement of first-order, horizontally beam-controlling loudspeaker cubes. In *e-Brief 447, 144th AES Conv.*, Milano, May 2018.

[7] A. M. Pasqual, P. Herzog, and J. R. Arruda. Theoretical and experimental analysis of the behavior of a compact spherical loudspeaker array for directivity control. *J. Acoust. Soc. Am.*, 128(6):3478–3488, 2010.

[8] A. M. Pasqual and V. Martin. On the acoustic radiation modes of compact regular polyhedral arrays of independent loudspeakers. *J. Acoust. Soc. Am.*, 130(3):1325–1336, 2011.

[9] M. Pollow and G. K. Behler. Variable directivity for platonic sound sources based on spherical harmonics optimization. *Acta Acustica united with Acustica*, 95(6):1082–1092, 2009.

[10] H. Pomberger. Angular and radial directivity control for spherical loudspeaker arrays. M. thesis, Institut für Elektronische Musik und Akustik, Kunstuni Graz, Technical University Graz, Graz, A, 2008.

[11] F. Schultz, M. Zaunschirm, and F. Zotter. Directivity and electro-acoustic measurements of the IKO. In *E-Brief 444, 144th AES Conv.*, May 2018.

[12] O. Warusfel, P. Derogis, and R. Causse. Radiation synthesis with digitally controlled loudspeakers. In *103rd AES Convention*, Paris, September 1997.

[13] F. Zotter and R. Höldrich. Modeling radiation synthesis with spherical loudspeaker arrays. In *Proceedings of the ICA*, Madrid, 02/09/2007 2007.

[14] F. Zotter, M. Zaunschirm, M. Frank, and M. Kronlachner. A beamformer to play with wall reflections: The icosahedral loudspeaker. *Computer Music Journal*, 41(3), 2017.

A CUBOID PISTON INTEGRALS

Integrating $\psi_{lmn}(\boldsymbol{x})$ over a disk, e.g., at $z = 0$, or $z = L_z$ of the radius R and centered at $x = a, y = b$, we get with scalars $\sqrt{(2-\delta_l)(2-\delta_m)(2-\delta_n)}\sqrt{L_x L_y L_z}^{-1}$ or $(-1)^n\sqrt{(2-\delta_l)(2-\delta_m)(2-\delta_n)}\sqrt{L_x L_y L_z}^{-1}$ excluded

$$\mathscr{I}_{\text{rect},\varphi,r} = \iint_{D(R,a,b)} \cos[\tfrac{\pi}{L_x}lx]\cos[\tfrac{\pi}{L_y}my]\,\mathrm{d}x\mathrm{d}y = \int_0^R \int_0^{2\pi} \cos[k_x(r\cos\varphi - a)]\cos[k_y(r\sin\varphi - b)]\,\mathrm{d}\varphi\,r\mathrm{d}r \quad (16)$$

By $\cos\alpha\cos\beta = \frac{\cos(\alpha+\beta)+\cos(\alpha-\beta)}{2}$ the term $\cos[k_x(r\cos\varphi - a)]\cos[k_y(r\sin\varphi - b)]$ becomes

$$\int_0^R \int_0^{2\pi} \tfrac{1}{2}[\cos(k_x r\cos\varphi + k_y r\sin\varphi - k_x a - k_y b) + \cos(k_x r\cos\varphi - k_y r\sin\varphi - k_x a + k_y b)]\,\mathrm{d}\varphi\,r\mathrm{d}r$$

where obviously we can gather the two sinusoids to one by $A\cos x + B\sin x = \sqrt{A^2 + B^2}\cos(x + \arctan\frac{B}{A})$ above, and essentially reformulate both expressions to $\cos[C\cos(x+D)+E]$ whose integral over x becomes

$$\int_0^{2\pi} \tfrac{1}{2}\cos[C\cos(x \pm D) + E \pm F]\,\mathrm{d}x = \cos(E \pm F)\tfrac{1}{\pi}J_0(A), \quad (17)$$

and therefore in sum $[\cos(E+F) + \cos(E-F)]\tfrac{1}{\pi}J_0(A) = \cos E \cos F \tfrac{2}{\pi}J_0(A)$. The inner integral in Eq. (16) is

$$\mathscr{I}_{\text{rect},\varphi} = \cos(\tfrac{\pi}{L_x}la)\cos(\tfrac{\pi}{L_y}mb)\tfrac{2}{\pi}J_0\big(r\pi\sqrt{(\tfrac{l}{L_x})^2 + (\tfrac{m}{L_y})^2}\big), \quad (18)$$

and is integrated $\int_0^R r\,\mathrm{d}r$; DLMF says $\int_0^x x J_0(x)\,\mathrm{d}x = x J_1(x)$, so $\int_0^R r J_0(kr)\,\mathrm{d}r = \frac{1}{k^2}\int_0^{kR} kr J_n(kr)\,\mathrm{d}kr = \frac{R}{k} J_1(kR)$,

$$\mathscr{I}_{\mathrm{rect},\varphi,\mathrm{r}} = \int_0^R \mathscr{I}_{\mathrm{rect},\varphi}\,r\,\mathrm{d}r = \cos(\tfrac{\pi}{L_x}l\,a)\cos(\tfrac{\pi}{L_y}m\,b)\,\frac{2RJ_1\left(R\pi\sqrt{(\frac{l}{L_x})^2+(\frac{m}{L_y})^2}\right)}{\sqrt{(\frac{l}{L_x})^2+(\frac{m}{L_y})^2}}. \tag{19}$$

B SPHERICAL MODE NORMALIZATION AND SMALL CAP

Orthogonality of the spherical Bessel functions fulfilling the boundary conditions $j_n'(\alpha) = j_n'(\beta) = 0$ is typically proven by inserting two different eigenvalues α, β, into the differential equation, and by integration over the spherical Bessel function with the respective other eigenvalue, yielding a difference of both equations

$$\alpha R\, j_n'(\alpha)\, j_n(\beta) - \beta R\, j_n(\alpha)\, j_n'(\beta) = \frac{-\alpha^2+\beta^2}{R^2}\int_0^R j_n(\tfrac{\alpha}{R}r)\, j_n(\tfrac{\beta}{R}r)\, r^2\,\mathrm{d}r. \tag{20}$$

Inserting $\alpha = k_{ln}R$ and $\beta = k_{l'n}R$ zeros the left side by the rigid condition $j_n'(k_{ln}R) = j_n'(k_{l'n}R) = 0$. With $l \neq l'$, the factor $-\alpha^2+\beta^2$ is non-zero so that the integral $\int_0^R j_n(\tfrac{\alpha}{R}r)\, j_n(\tfrac{\beta}{R}r)\, r^2\,\mathrm{d}r = 0$ must be zero, verifying the orthogonality of $j_n(k_{ln}r)$ and $j_n(k_{l'n}r)$. The integral needn't vanish for $l = l'$: its factor $-\alpha^2+\beta^2 = 0$ vanishes. We also need to know the missing normalization term N_{ln}, which we find by multiplying Eq. (20) with $\frac{R^2}{\beta^2-\alpha^2}$ and setting $\beta = k_{ln}R$, so that $j_n'(\beta) = 0$

$$\frac{1}{N_{ln}^2} = \lim_{\alpha\to\beta}\int_0^R j_n(\tfrac{\alpha}{R}r)\, j_n(\tfrac{\beta}{R}r)\, r^2\,\mathrm{d}r = \lim_{\alpha\to\beta}\frac{\beta\, j_n(\alpha)\, j_n'(\beta) - \alpha\, j_n'(\alpha)\, j_n(\beta)}{\alpha^2-\beta^2}R^3\Big|_{\beta=k_{ln}R} = \lim_{\alpha\to\beta}\frac{-\alpha\, j_n'(\alpha)\, j_n(\beta)}{\alpha^2-\beta^2}R^3.$$

Letting $\alpha \to \beta$, we get a $\frac{0}{0}$ expression as $\lim_{\alpha\to\beta} j_n'(\alpha) = 0$. We derive numerator and denominator (de l'Hopital) with regard to α and get

$$\frac{1}{N_{ln}^2} = \lim_{\alpha\to\beta}\frac{[-j_n'(\alpha)-\alpha j_n''(\alpha)]j_n(\beta)}{2\alpha}R^3 = \lim_{\alpha\to\beta}\frac{[-\alpha j_n'(\alpha)-\alpha^2 j_n''(\alpha)]j_n(\beta)}{2\alpha^2}R^3. \tag{21}$$

The spherical Bessel differential equation helps simplifying $-\alpha^2 j_n''(\alpha) = 2\alpha j_n'(\alpha) + [\alpha^2 - n(n+1)]j_n(\alpha)$

$$\frac{1}{N_{ln}^2} = \lim_{\alpha\to\beta}\frac{\{\alpha j_n'(\alpha)+[\alpha^2-n(n+1)]j_n(\alpha)\}j_n(\beta)}{2\alpha^2}R^3 = \frac{[\beta^2-n(n+1)]j_n^2(\beta)}{2\beta^2}R^3 = \frac{[1-\frac{n(n+1)}{\beta^2}]j_n^2(\beta)R^3}{2}, \tag{22}$$

which is verified by the indefinite integral $\int j_n(kr)\, r^2\,\mathrm{d}r = \frac{r^3}{2}[j_n^2(kr) - j_{n-1}(kr)j_{n+1}(kr)]$ using $j_{n-1} = j_n' + \frac{n+1}{x}j_n$ and $j_{n+1} = -j_n' - \frac{n}{x}j_n$, where for $k = k_{ln}$ only $-\frac{n(n+1)}{x^2}j_n^2$ remains as j_n' vanishes. The exceptional constant mode $\beta \to 0$ for $n = 0$ is not allowed above, but $j_0(0) = 1$ makes it easily solved $\frac{1}{N_{00}^2} = j_0^2(0)\int_0^R r^2\,\mathrm{d}r = \frac{j_0^2(0)R^3}{3}$, so that

$$N_{ln}^2\, j_n^2(k_{ln}R)\, R^3 = \begin{cases} 2\frac{(k_{ln}R)^2}{(k_{ln}R)^2-n(n+1)}, & \text{unless } k_{ln} = 0 \\ 3, & \text{for } k_{ln} = 0,\ \text{i.e. } n = l = 0. \end{cases} \tag{23}$$

Small-cap approximation Using $P_n(1) = 1$ and $P_n'(1) = \frac{n(n+1)}{2}$ yields $\lim_{\Delta x\to 0} P_n(1-\Delta x) = 1 - \frac{n(n+1)}{2}\Delta x$ with $\Delta x = 1 - \cos\frac{\alpha}{2}$, here α denotes the aperture, to approximate the cap weights

$$a_n = 2\pi\int_{\cos\frac{\alpha}{2}}^1 P_n(x)\,\mathrm{d}x = -2\pi\frac{P_{n+1}(\cos\frac{\alpha}{2})-\cos\frac{\alpha}{2}P_n(\cos\frac{\alpha}{2})}{n} = 2\pi\frac{P_{n-1}(\cos\frac{\alpha}{2})-P_{n+1}(\cos\frac{\alpha}{2})}{2n+1}, \tag{24}$$

$$\text{by } \lim_{\alpha\to 0} a_n = 2\pi\frac{-(n-1)n\Delta x + (n+1)(n+2)\Delta x}{2(2n+1)} = 2\pi\frac{2(2n+1)}{2(2n+1)}\Delta x = 2\pi(1-\cos\tfrac{\alpha}{2}). \tag{25}$$